Composite Structures 143 (2016) 103–116

Contents lists available at ScienceDirect

Composite Structures

journal homepage: www.elsevier.com/locate/compstruct

# Computational modeling of carbon/carbon composites under thermal shock conditions

Alma L. Leanos, Pavana Prabhakar *

*Department of Mechanical Engineering, University of Texas at El Paso, El Paso, TX 79968, USA*

ARTICLE INFO

*Article history:*
Available online 12 February 2016

*Keywords:*
Carbon–carbon composite
Compressive stiffness degradation
Computational model
Oxidation
Carbon decomposition

ABSTRACT

The influence of thermal shock conditions on the extent of carbon material decomposition and through-thickness compressive stiffness degradation of 2D woven carbon/carbon (C/C) composites is predicted by computational efforts and validated against experimental results. The proposed computational framework consists of two main steps: (a) radiation heat transfer analysis on a meso-scale C/C composite model exposed to thermal shock conditions accounting for the heat flux due to decomposing material; (b) stress analysis to model the carbon stiffness degradation due to oxidation observed in the previous step. This is followed by a through-thickness compression analysis on the meso-scale model to determine the composite compressive stiffness. The predicted oxidation behavior and compressive responses of the meso-scale model under various thermal shock conditions are in good agreement with previously published experimental results for temperatures up to 700 °C. Therefore, the proposed computational framework can be used in the initial design of C/C composites and thermal protection systems. That is, it can potentially be used for modeling other C/C composites by changing the fiber architecture, weave pattern and/or fiber volume fraction.



## 1. Introduction

### 1.1. C/C composites

Material scientists and structural engineers working in the aerospace and nuclear industries have a great interest in exploring materials that can sustain high temperatures (in the range of 800–1000 °C) in oxidizing environments [1]. Carbon–carbon (C/C) composites, which consist of carbon fibers reinforced in carbon matrix, have the capacity to retain exceptional thermal and mechanical properties at high temperatures (e.g., 3000 °C) in inert atmospheres [2]. Therefore, C/C composites are desirable for high temperature structural applications. Several earlier researchers [3–12] have experimentally explored the properties of C/C composites at room temperature and high temperatures in inert conditions. However, the mechanical properties of C/C composites in oxidizing environments [13–15], both at room and high temperatures, have seldom been studied. That is, properties like low density, high specific modulus and strength, high thermal conductivity, small coefficient of thermal expansion, high toughness and high thermal and ablation resistance of C/C composites at high temperatures in non-oxidizing environments [8,16] are well known. However, C/C composites appear to degrade rapidly at temperatures as low as 450 °C in oxidizing environments [17], although their mechanical properties improved or maintained at high temperatures in inert conditions [18]. Nonetheless, C/C composites with effective surface protection systems are potential candidates for use in high temperature applications, such as, reentry rocket nose cone, solid rocket motor (SRM) nozzle throats, missile nose-tips and leading edges [19,20], as well as defense specific applications that require explosion-resistant structural parts. However, the integrity of a structure can be adversely affected by thermal shock exposure in oxidizing environments due to the ablation of carbon materials.

### 1.2. Oxidation of C/C composites

In this paper, the influence of oxidation on the through-thickness compression of C/C composites is computationally investigated. An experimental investigation of the stiffness degradation and corresponding oxidation mechanisms of 2D C/C composites under thermal shock conditions in an oxidizing environment has been previously reported by the authors [15]. Experimental exploration of the effects of oxidation on C/C composites is complicated and expensive with varying weave pattern, carbon materials, microstructure and processing condition of the composite [21–23],

* Corresponding author. Tel.: +1 915 747 5863.
*E-mail address:* pprabhakar@utep.edu (P. Prabhakar).

http://dx.doi.org/10.1016/j.compstruct.2016.02.017
0263-8223/

which possesses a necessity for developing computational frameworks to understand and predict the thermal response and material degradation of C/C composites. Such a framework has the potential to aid the initial design process and maintain protection systems for quality and reliability of the structural parts throughout their expected life-time.

High temperature exposure in oxidizing environments can cause a combination of physical, chemical, thermal, mechanical and structural changes in fiber-reinforced polymer (FRP) composites [24] that present extreme challenges to model and capture all these material changes simultaneously. Typically, computational frameworks are restricted to one or two changes only, like, thermo-chemical or thermo-physical studies. Coupling these models to predict mechanical response can result in thermo-mechanical modeling frameworks.

Few computational models have been developed to analyze the oxidation behavior of C/C composites. A micromechanical model of 3D C/C composites at high temperatures was developed by Liu and Yang [16] to analyze the damage morphology of the constituents. A 1D diffusion model to describe surface ablation recession of C/C composites was performed by Aspa et al. [25]. Further, the surface roughness due to oxidation of C/C composites was analyzed by Vignoles et al. [26] and Lachaud et al. [27] using 3D reaction–diffusion local models. Laborde et al. [28] developed a damage model for C/C composites accounting for the thermo-mechanical effects into their numerical solution.

In the current paper, a thermo-chemo-mechanical model is developed that is capable of predicting the degree of decomposition of carbon material under thermal shock conditions in oxidizing environments, which is followed by the prediction of through-thickness stiffness of 2D C/C composites. The predictions are compared against the experimental results previously reported by Leanos and Prabhakar [15].

## 2. Material description and properties

In general, manufacturing processes, like, solid pyrolysis using thermosetting resins, pitch route using liquid infiltration carbonization, chemical vapor deposition (CVD), etc. are used to fabricate ceramic matrix composites (CMCs). The 2D woven C/C composite modeled in this paper was fabricated using liquid pitch processing route (purchased from Bay Composites Inc., USA), which typically results in a porous structure impregnated with liquid phase pitch/phenolic resin, followed by carbonization and high temperature treatment (approx. 1000–2700 °C) [18].

The composite consists of 10 layers/lamina of reinforcement that are vacuum densified with phenolic resin as matrix precursor and exposed to a final heat treatment temperature of 1100 °C. Each lamina is constructed in a $2 \times 2$ direct twill weave pattern by interweaving longitudinal and transverse tows made of approximately 6000 polyacrilonitrile (PAN) carbon fibers each. The fiber volume fraction ('$V_f$') within a tow is $\approx 79 \pm 1.5\%$, which is an input for predicting the carbon tow properties. Several greyscale images of the transverse cross-section within the tow regions of the C/C composite specimens at the micro-scale are captured (Fig. 1)) and transformed to binary images using Matlab (Fig. 1(b)). The contrast of the fibers and matrix regions is used to determine the percentage area of fibers within the tows. The fiber volume fraction within a tow is then calculated as the area occupied by the fibers with respect to the total area of the image, and is repeated for several images to obtain a distribution of the $V_f$ value.

Thermal properties of carbon fibers and matrix are obtained from the literature [29] and are listed in Table 1. Moreover, the properties of the constituent materials and their corresponding fiber volume fractions are used to determine the thermal conductivities '$k$' of a tow (subscript '$t$') in the longitudinal (superscript '*long*') and transverse (superscript '*trans*') directions [24,30], as:

$$k_t^{long} = k_f^{long} V_f + k_m V_m; \quad k_t^{trans} = \frac{k_f^{trans} k_m}{k_f^{trans} V_f + k_m V_m} \tag{1}$$

where, subscripts '$f$' and '$m$' denote the fiber and matrix, respectively. Table 1 lists the computed tow properties. Similarly, the rule of mixtures is used to obtain the density '$\rho$' and specific heat capacity '$C_p$' for a tow as:

$$\rho_t = \rho_f V_f + \rho_m V_m; \quad C_{pt} = C_{pf} V_f + C_{pm} V_m \tag{2}$$

Carbon fiber elastic properties (shown in Table 2) are obtained from Pardini and Gregori [31]. The carbon matrix properties are assumed such that the pristine C/C composite compressive stiffness obtained from the proposed computational model matches the pristine compressive stiffness obtained experimentally in Leanos and Prabhakar [15] (i.e., ≈1.74 GPa). Concentric cylinder model (CCM) equations, which require the constituents properties and fiber volume fraction, are used to determine the tow elastic properties. Here, subscript '1' corresponds to the tow direction, and '2' and '3' correspond to the plane perpendicular to the '1' direction.

According to Bai et al. [24], C/C composites are considered to be porous structures such that gas can be stored or propagated through the pores. Thus, the variation of the density '$\rho_i$' and thermal conductivity '$k_i$' with the amount of weight loss '$\alpha$' is assumed to vary linearly as:

$$\rho_i = \rho_b(1-\alpha) + \alpha\rho_a; \quad k_i = k_b(1-\alpha) + \alpha k_a \tag{3}$$

where, subscripts '$b$' and '$a$' denote properties before degradation (i.e., when $\alpha$=0) and after complete degradation (i.e., $\alpha = 1$), respectively. The properties before degradation are those shown in Table 1, while the density and thermal conductivity after degradation for both the tow and carbon matrix are assumed to be '$\rho_a = 10$ kg/m$^3$' and '$k_a = 0.01$ W/m.K', respectively.

## 3. Brief description of previous experimental work

Oxidation mechanisms and through-thickness stiffness degradation of 2D C/C composite specimens exposed to oxidizing environments were experimentally analyzed and reported in a previous work by Leanos and Prabhakar [15]. The 2D C/C composite plate described in Section 2 had an average thickness of 5.25 mm and was sectioned into square specimens with sides about 12.7 mm. These test specimens were placed in a ceramic boat that was further positioned into a heating furnace (Model BF51766A-1 Lindberg/Blue M, Thermo Fisher Scientific, Inc., USA) and exposed to thermal shock conditions with peak temperatures ranging from 400 °C to 1000 °C. Following this, through-thickness compression tests were performed on pristine and thermally exposed test specimens using a servo–hydraulic fatigue testing system (Model 8801, Instron Corporation, USA) to determine their compressive responses. The through-thickness stiffness measured after each thermal shock condition was compared against the pristine stiffness (≈1.74 GPa). It was established that the compressive mechanical response degrades with increasing thermal shock peak temperature starting at ≈400 °C in oxidizing environments. Further, it was also concluded that the carbon matrix degrades much faster than the carbon fiber tows during an ablation process and an apparent change in oxidation mechanism occurs around 600 °C.

## 4. Computational framework

A novel computational modeling methodology to predict the stiffness degradation due to oxidation is developed in the current

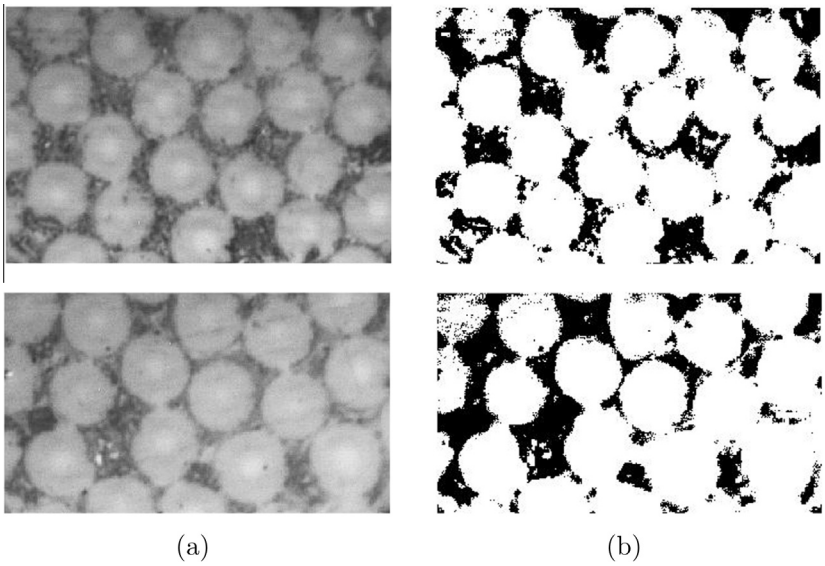


**Fig. 1.** Micro-scale images of fibers within tows: (a) greyscale images and (b) binary images from matlab.

**Table 1**
Thermal properties of C/C composite constituent materials.

| Material | k (W/m.K) | $\rho$ (kg/m$^3$) | $C_p$ (J/kg.K) |
|---|---|---|---|
| Carbon fiber transverse | 4 | 1928 | 9.21e−4 |
| Carbon fiber longitudinal | 40 | 1928 | 9.21e−4 |
| Carbon matrix | 10 | 1800 | 7.17e−4 |
| Carbon tow transverse | 7.7 | 1902 | 8.80e−4 |
| Carbon tow longitudinal | 34 | 1902 | 8.80e−4 |

**Table 2**
Elastic properties of C/C composite constituent materials.

| Elastic property | Carbon fiber | Carbon matrix | Carbon fiber tow |
|---|---|---|---|
| $E_{11}$(MPa) | 230*e*3 | 0.64*e*3 | 1.8412*e*5 |
| $E_{22} = E_{33}$(MPa) | 20*e*3 | 0.64*e*3 | 3.09*e*3 |
| $G_{12} = G_{13}$(MPa) | 12*e*3 | 0.246*e*3 | 1.8744*e*3 |
| $G_{23}$(MPa) | 9.7*e*3 | 0.246*e*3 | 1.5204*e*3 |
| $\nu_{12} = \nu_{13}$ | 0.18 | 0.3 | 0.1985 |
| $\nu_{23}$ | 0.0283 | 0.3 | 0.0162 |

investigation. The finite element framework was developed using a commercially available software (ABAQUS) with additional user subroutines to capture the complex physics during oxidation. The proposed computational model is able to simulate the oxidation behavior of the 2D C/C composite specimens exposed to the experimental conditions described in Section 3. Also, the proposed scheme is verified by comparing the predicted through-thickness compressive stiffness of the 2D C/C composite specimens to that obtained experimentally by Leanos and Prabhakar [15].

Fig. 2 shows a schematic of the computational procedure, which consists of two main steps: (1) Step 1 – a radiation heat transfer analysis to determine the temporal and spatial distribution of temperature and material weight loss; (2) Step 2 – a stress analysis to determine the through-thickness compressive stiffness of the C/C composite. Primary inputs to the computational model are the thermogravimetric analyses (TGA) curves of the composite and its constituents. The following sub-section describes the oxidation kinetic input parameters necessary for Step 1 of the computational framework.

### 4.1. Oxidation kinetics

Kinetic parameters are required as inputs to the proposed computational framework as they describe the degree of decomposition of carbon materials (i.e., fiber tow and matrix) under thermal shock conditions in air. Generally, the constituent materials degrade and experience different types of oxidation mechanisms upon exposure to these conditions, i.e., linear, parabolic and logarithmic-rate reactions [16]. During the linear stage, weight loss of the composite follows the expression given by Guo et al. [32]:

$$K(T) = \frac{d\alpha}{dt} \tag{4}$$

where, '$K(T)$' is the oxidation rate constant depending on the temperature '$T$', '$\alpha$' is weight loss and '$t$' is the time. Further, this equation follows the Arrhenius equation:

$$lnK(T) = lnA - \frac{E}{RT} \tag{5}$$

where, '$A$' is the pre-exponential factor, '$E$' is the activation energy and '$R$' is the gas constant ($R = 8.314e3$ mJ(K mol)$^{-1}$). The Arrhenius kinetic parameters (i.e., '$A$' and '$E$') may vary with temperature and the amount of weight loss, as summarized by Guo et al. [32]. Vyazovkin and Wight [33] investigated the variation of kinetic parameters and stated that the oxidation of 2D C/C composites might need to be decomposed into two or more single-step processes. That is, the variation of kinetic parameters with temperature ranges might be attributed to a change in oxidation mechanism, as observed experimentally by Leanos and Prabhakar [15].

Section 5 describes the experimental approach to determine the TGA curves and their post-processing to extract the oxidation kinetic parameters. Section 6 provides the same for steady state air flow condition, which resembles the experiments reported in Leanos and Prabhakar [15]. Thus, the kinetic parameters determined in Section 6 are used as inputs to Step 1 of the computational framework. Section 7 provides details of the meso-scale model geometry and architecture of the 2D twill pattern C/C composite. Radiation heat transfer analysis conducted on the meso-scale model in Step 1 is described in Section 8. The temporal and spatial distribution of temperature and material weight loss from Step 1 is then imported as inputs to the stress analysis described

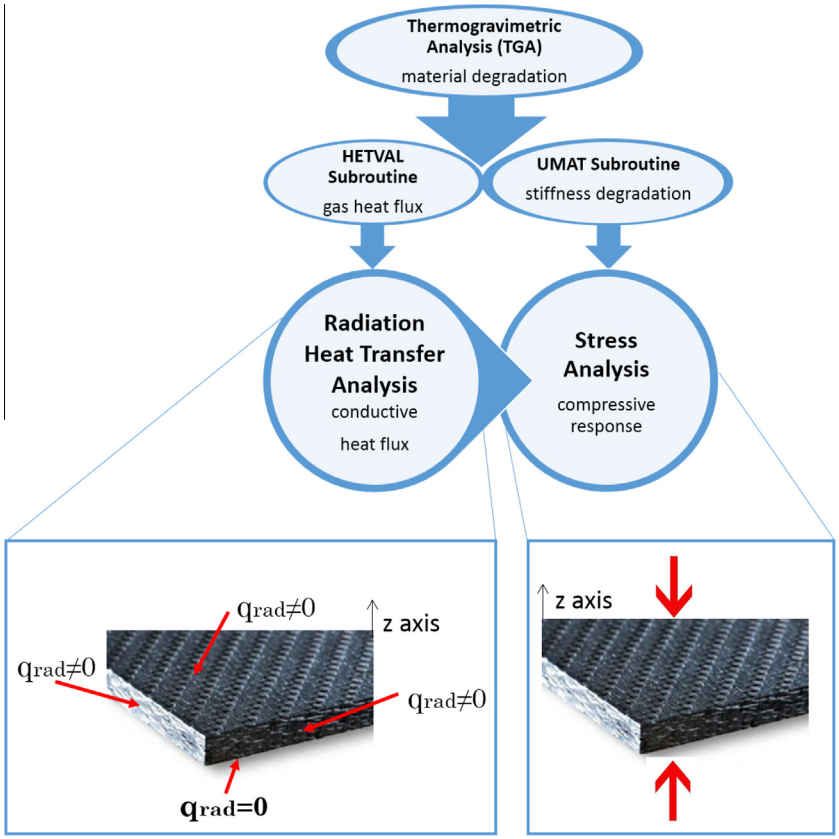


**Fig. 2.** Schematic representation of the procedure followed by the proposed computational framework.

in Section 9 (Step 2). In Step 2, material weight loss and temperature distribution are related to stiffness degradation to determine the through-thickness compressive stiffness of the C/C composite.

## 5. Thermogravimetric analysis

Several researchers have reported thermogravimetric analyses (TGA) in oxidizing environments previously with varying air flow rate, pressure, temperature, thermal cycle, etc. among other experimental conditions [34–45]. For example, Guo and Xiao [34] performed isothermal TGA on carbon felt/carbon composites by exposing them to flowing air at 50 ml/min. Similarly, Park and Seo [35] performed isothermal TGA on unidirectional C/C composites under flowing air. In this paper, TGA are performed on C/C composite specimens and carbon fibers using a thermogravimetric analyzer (Netzsch TGA 209 F1 Iris). The weight loss of C/C composite specimens and carbon fibers are captured as a function of time during isothermal oxidation in an Oxygen-Argon environment at 400 °C, 600 °C, 700 °C and 800 °C. Square test specimens with sides of $4 \pm 0.11$ mm are sectioned from the composite plate for the TGA, resulting in an average volume '$Vol_{comp}$' of 84 mm$^3$. Likewise, carbon fibers are cut from a carbon fiber textile that consists of carbon fiber tows interwoven together. The initial mass '$M$' of the carbon fiber samples are 20.65 mg, 24.17 mg, 24.84 mg and 11.8 mg for the 400 °C, 600 °C, 700 °C and 800 °C isothermal conditions, respectively. The specimens are placed in alumina crucibles with diameter of 5.85 mm during the analysis and are heated to the desired temperature (400 °C, 600 °C, 700 °C and 800 °C) for isothermal oxidation in 99.99% Argon air at a flow rate of 50 ml/min. Upon reaching the desired temperature, the specimens are held for 5 min under the same condition. Following this, the specimens are heated at a constant temperature in an air mixture of 20% Oxygen and 80% Argon at flow rates of 10 ml/min and 40 ml/min, respectively, such that the total air flow reaches 50 ml/min.

All external surfaces of the specimens except the bottom are exposed to flowing air, maximizing the area of contact with the oxidizing medium. The recorded weight loss '$\alpha$' is normalized such that '$\alpha = 1$' represents complete degradation of the specimen due to isothermal oxidation and '$\alpha = 0$' refers to the pristine specimen (i.e., unoxidized). Weight loss vs time (TG curves) for the C/C composite specimens and carbon fibers are shown in Fig. 3a) and Fig. 3 (b), respectively.

### 5.1. Post-processing of TG curves

Thermogravimetric curves for the C/C composite specimens and carbon fibers are post-processed to predict the fiber tow and matrix TG curves that provide the input kinetic parameters to the computational framework. In summary, these parameters define the weight loss within a composite unit cell '$\alpha_{comp}$' under thermal shock conditions in air from the weight loss behavior of the carbon matrix '$\alpha_m$' and fiber tow '$\alpha_t$' as:

$$\alpha_{comp} = \alpha_t V_{tc}^{mod} + \alpha_m V_{mc}^{mod} \tag{6}$$

where '$V_{tc}^{mod}$' and '$V_{mc}^{mod}$' are the volume fraction of the fiber tow and matrix within a composite unit cell, respectively.

It can be observed in Fig. 3a) and (b) that the time taken by the composite specimens to degrade completely is very large compared to that of the individual carbon fibers. This is due to higher average volume of composite specimens as compared to carbon fiber samples. Therefore, carbon fiber sample must have the same volume as the average volume of the composite specimens

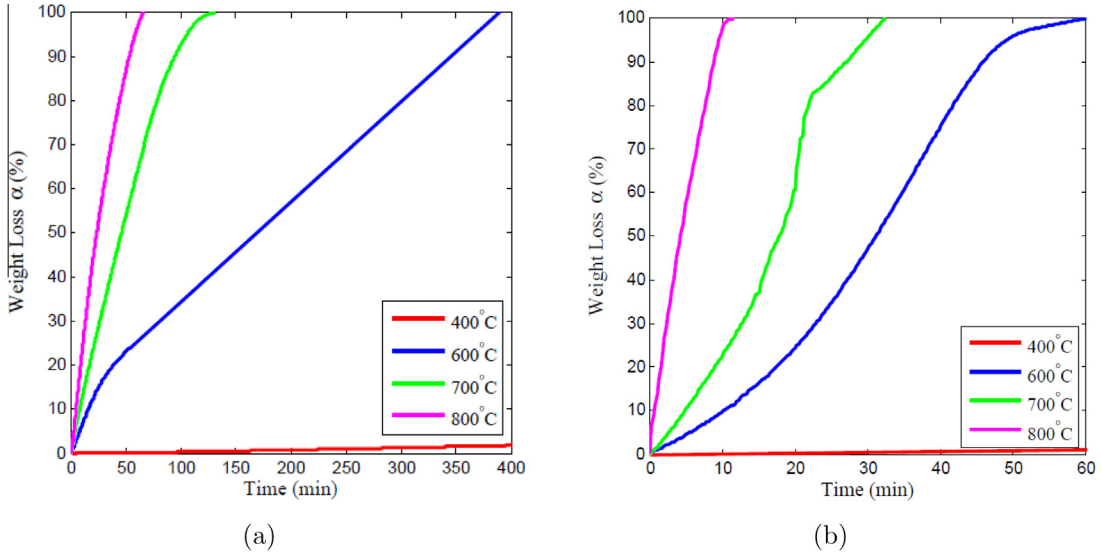


**Fig. 3.** TG curves upon exposure to different constant temperatures in Air at 50 ml/min for (a) C/C composite and (b) carbon fibers.

to compare the corresponding TG curves. To make the TG curves comparable, the oxidation time of each carbon fiber TG curve '$t_{fiber}$' is modified using the following:

$$t_{fiber}^{new} = t_{fiber} * C \tag{7}$$

where, '$C$' is a constant and the superscript '*new*' represents the new time that is utilized to define the new carbon fiber TG curve for each isothermal condition. The volume of the carbon fiber samples '$Vol_{fiber}$' is determined from the density '$\rho$' of the carbon fibers (refer to Table 1) and their mass '$M$' as $Vol_{fiber} = \frac{M}{\rho}$, where '$Vol_{fiber}$' is calculated for each isothermal condition. The constant '$C$' is then determined as:

$$C = \frac{Vol_{comp}}{Vol_{fiber}} \tag{8}$$

Values of '$C$' for each isothermal condition are shown in Table 3, and Eq. 7 is utilized to modify the oxidation time of the TG curves for the carbon fiber sample (shown in Fig. 3(b)), while the weight loss behavior is unaltered as shown in Fig. 4(a). Besides this, a time relation among Fig. 3a) and Fig. 4(a) for the total degradation times can be found as:

$$t_{fiber}^{end} = t_{comp}^{end} * D \tag{9}$$

where, the superscript '*end*' indicates the last time measurement recorded for each isothermal condition (i.e., when $\alpha = 1$) and '$D$' is a constant, as shown in Table 4. The fiber oxidation time for each isothermal condition can be predicted using this relation from any composite TG curves without the need of performing physical experiments. This prediction is based on the assumption that the fiber oxidation time varies with the volume of the fiber samples, however, the oxidation behavior (i.e., weight loss) remains the same. This assumption is important as it reduces the number of required experiments to only those performed on the composite specimens, while the fiber, matrix and fiber tow TG curves are predicted.

**Table 3**
Constant 'C' to determine the fiber TG curve for each isothermal condition.

| Isothermal temperature | 400 °C | 600 °C | 700 °C | 800 °C |
|---|---|---|---|---|
| '$C$' value | 7.84 | 6.7 | 6.52 | 13.73 |

Fiber volume fraction within the meso-scale C/C composite unit cell '$V_{fc}$' is required to predict the matrix and tow TG curves. The volume fraction of the fiber tows '$V_{tc}^{mod}$' within the meso-scale unit cell is approximately determined to be equal to 64%, while that for the matrix '$V_{mc}^{mod}$' is approximately 36%. However, a carbon fiber tow itself comprises of 80% of individual fibers '$V_f$' and 20% of matrix '$V_m$' (from the fiber volume fraction within a tow). Therefore, the total fiber volume fraction within the composite '$V_{fc}$' is determined to be ≈51.2% and the total matrix volume fraction '$V_{mc}$' ≈48.2%.

Hence, the matrix TG curves are predicted using the following rule of mixtures, as:

$$\alpha_{comp} = \alpha_f V_{fc} + \alpha_m V_{mc} \tag{10}$$

Rearranging the above equation, the matrix weight loss behavior is determined as:

$$\alpha_m = \frac{\alpha_{comp} - \alpha_f * 0.512}{0.482} \tag{11}$$

Similarly, the fiber tow TG curves can also be predicted from the rule of mixtures as:

$$\alpha_t = \alpha_f V_f + \alpha_m V_m \tag{12}$$

As a result, the amount of weight loss of a meso-scale C/C composite unit cell is predicted from the matrix and fiber tow TG curves by satisfying Eq. 6. For example, at any given time, the summation of the fiber tow and matrix weight loss must match the composite weight loss, as shown in Fig. 4(b).

### 5.2. Oxidation kinetic parameters

First, in order to verify the TG results of the C/C composite (i.e., linear stage of Fig. 3(a)), the oxidation rate constants '$K(T)$' are calculated for different temperatures and compared to those reported by Park and Seo [35] and Guo and Xiao [34] for a unidirectional C/C composite and a carbon felt/carbon composite, respectively (see Fig. 5(a)). Fig. 5(a) shows the oxidation Arrhenius curves for comparison, where it is illustrated that the C/C composite oxidation (red line) consists of two stages separated at a temperature about 700 °C to support a change in oxidation mechanism at this temperature. Activation energies that refer to the slopes of the oxidation curves are then calculated for different temperatures

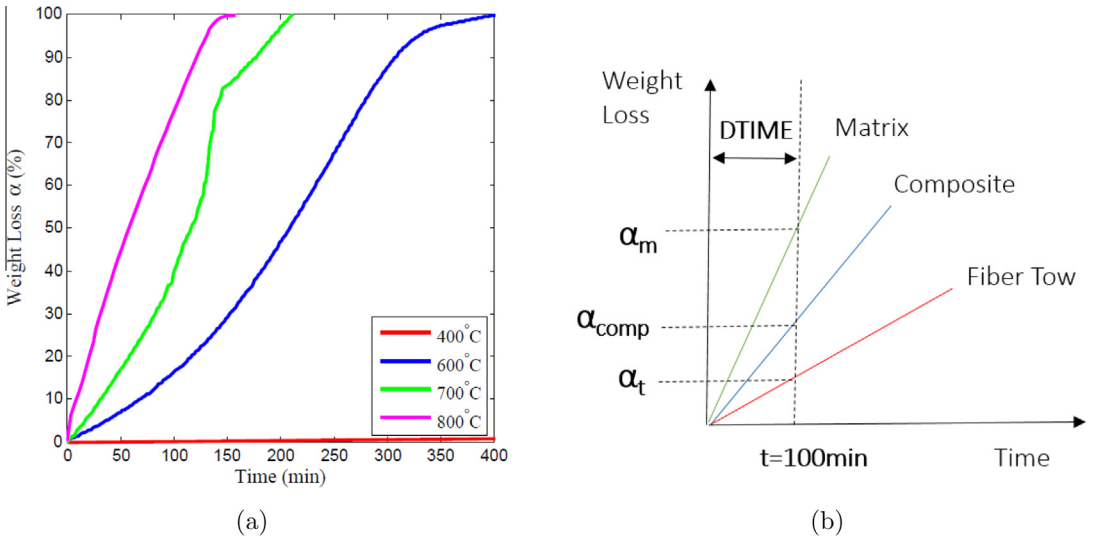


**Fig. 4.** (a) Comparable TG curves for carbon fibers upon exposure to different constant temperatures in air at 50 ml/min and (b) schematic representation of the prediction of composite TG curves from fiber tows and matrix TG curves.

**Table 4**
Constant 'D' to define a relation between fiber and composite TG curves for each isothermal condition.

| Isothermal temperature | 400 °C | 600 °C | 700 °C | 800 °C |
|---|---|---|---|---|
| '*D*' value | 2.07 | 1.031 | 1.62 | 2.39 |

**Table 5**
Comparison of activation energy between the C/C composite and other carbon composites assuming linear oxidation stage.

| Activation energy $E$(mJ $*$ mol$^{-1}$) | 600–700 °C | 700–800 °C |
|---|---|---|
| C/C composite | 4.26e7 | 6.67e7 |
| Unidirectional C/C composite [35] | 3.3e7 | 3.3e7 |
| Carbon felt/carbon composite [34] | – | 10.12e7 |

and compared in Table 5. It can be observed that at low temperatures (i.e., from 600 °C to 700 °C), the C/C composite oxidation curve (red line) possesses very similar oxidation behavior (i.e., activation energy '*E*') to that of a unidirectional C/C composite (black line). In this case, the activation energy varies about 22% due differences in the unidirectional C/C composite fiber volume fraction (60%), crucible utilized in the experiment (platinum wire cage) and air flow conditions as compared to those reported in this paper. On the other hand, the activation energy of the C/C composite at high temperatures (i.e., from 700 °C to 800 °C) is found to be between the carbon felt/carbon composite and unidirectional C/C composite activation energies. However, it can be observed that once the conversion temperature (i.e., 700 °C) is reached, the C/C composite oxidation rates are comparable to that of a carbon felt/carbon composite. Therefore, it is suggested that for this range of temperatures, the C/C composite oxidation behavior (red line) is best resembled by that of a carbon felt/carbon composite (blue line). Variation of activation energies between the composites might be caused by differences in carbon felt/carbon composite samples' volume (21 mm$^3$) and constituents' material properties (i.e., density and strength). Further details about kinetic parameters and comparisons with the literature are discussed in Section 6.2.

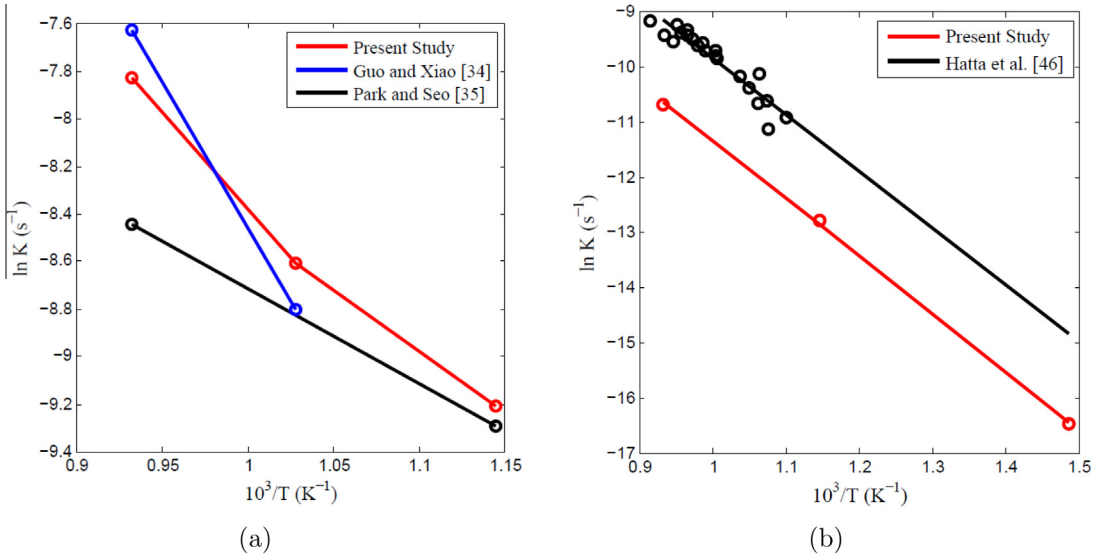


**Fig. 5.** Comparison of Arrhenius plots of oxidation for different composites assuming linear oxidation stage for (a) flowing air and (b) steady air conditions.

Following this, the kinetic parameters for the carbon tow and matrix are determined, and the compressive stiffness of the C/C composite unit cell under various thermal shock conditions is predicted and further compared to experimental results. The maximum percentage difference between experimental and predicted results is found to be about 80% for the 800 °C thermal shock condition. Since, the percentage difference is very large and the conversion temperature is not in good agreement with Leanos and Prabhakar [15], it is concluded that the current air flow condition does not simulate the experimental conditions accurately and further TG experiments need to be performed for steady air conditions, as discussed in the next section.

## 6. Thermogravimetric analysis for steady air conditions

The oxidation kinetics of carbon composites under steady air flow conditions are less known. Hatta et al. [46] analyzed isothermal TGA on 2D C/C composites under natural convection of air, which can be treated as steady air flow. In the article by Leanos and Prabhakar [15], the C/C composite specimens are exposed to thermal shock conditions using a heating furnace at a very small air flow rate (i.e., almost steady). In order to best resemble these experimental conditions, C/C composite specimens are exposed to TGA under steady air conditions. However, performing these experiments is extremely time consuming. Therefore, the fiber, fiber tow and matrix TG curves are predicted using the relations obtained in Section 5.1. It is assumed that the calculated '*D*' values can be used for different air flow conditions.

As explained in the previous section, only the TG curves of the C/C composite specimens are now required to predict all the inputs to the computational framework. In this section, TGA is performed on C/C composite specimens using a thermogravimetric analyzer (Severn Solutions Ltd) that is able to perform oxidation tests at steady air flow conditions. All the experimental conditions are held the same as those in Section 5, except that the C/C composite specimens are now heated at a constant temperature (i.e., 400 °C, 600 °C and 800 °C) in steady air during which the weight loss is captured as a function of time. In other words, upon reaching a desired temperature, Argon supply is stopped and air starts flowing from the exterior to the heating chamber at a steady flow rate, resembling the heating furnace conditions described by Leanos and Prabhakar [15]. The weight loss vs. time (TG curves) for the C/C composite specimens are shown in Fig. 6.

### 6.1. Post-processing of TG curves for steady air conditions

The assumptions and equations described in Section 5.1 are utilized to determine the carbon fiber, fiber tow and matrix TG curves from the TG experiments with steady air flow as the oxidizing medium. The fiber sample oxidation time (Fig. 7(a)) is predicted from Eq. 9, while the weight loss behavior is the same as Fig. 3 (b). It can be observed in Fig. 7(a) that all the TG curves are linear before a critical time '$t_{cr}$' equal to 745 min. Therefore, the matrix TG curves are predicted up to this critical time from Eq. 11 and are shown in Fig. 7(b).

With this information, the TG curves for the carbon fiber tows can be constructed using Eq. 12 as shown in Fig. 8(a). It is important to notice that the rule of mixtures described by Eq. 6 is satisfied at any given time. Finally, the matrix and fiber tow TG curves are utilized to determine the oxidation kinetic parameters described in the following section.

### 6.2. Oxidation kinetic parameters for steady air flow conditions

In the current work, the carbon fiber tow and matrix weight loss behavior are found to be linear before a critical time '$t_{cr}$' equal to 745 min, which are utilized to develop the following kinetic analysis. First, in order to verify the TG results of the C/C composite (i.e., linear stage of Fig. 6), the oxidation rate constants '$K(T)$' are determined for different temperatures and compared to the oxidation data reported by Hatta et al. [46] for a 2D C/C composite. The corresponding oxidation rate constants are fitted along a least-squares line for comparison, as illustrated in Fig. 5(b). This figure shows that the slopes of both oxidation Arrhenius curves are very similar (i.e., oxidation behavior/activation energy '*E*'). However, small variations in oxidation rates might be attributed to different experimental conditions as compared to those presented in this paper, for example, the samples' volume (2700 $mm^3$), fiber volume fraction (50%), fabrication process, stacking sequence (0 °C/90 °C), heat treatment temperature (2073 K) and TGA equipment (Xenon lamp heating).

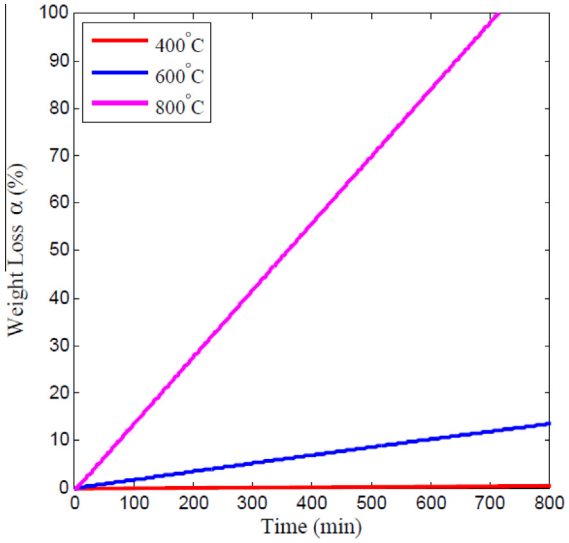


**Fig. 6.** TG curves for C/C composite specimens upon exposure to different constant temperatures in steady air.

Assuming that both C/C composites experience a single-step process through the whole range of temperatures during oxidation, kinetic parameters '*A*' and '*E*' can be obtained from Eq. 5 via linear regression as '$y = mx + b$', where '*y*', '*m*', '*x*' and '*b*' correspond to the terms '$lnK(T)$', '$-E/R$', '$1/T$' and '$lnA$' of Eq. 5, respectively. Table 6 summarizes each set of kinetic parameters, showing very similar activation energy '*E*' between the composites (i.e., 1.83% difference). Thus, it is suggested that both composites require comparable amount of energy to generate physical, thermal and/or chemical changes in the material (i.e., to react with the oxidizing medium) [15,47–49].

In addition, other researchers have explored the oxidation behavior of carbon composites and reported their corresponding activation energies [43,50–52,44,53]. Han et al. [43] reported an activation energy of '$E = 8.75e7$ mJ$(mol)^{-1}$' for a 3D C/C composite exposed to temperatures in the range of 650–800 °C. Cheng et al. [50] analyzed the oxidation behavior of a C/C composite with a three-layer coating for temperatures below 700 °C and reported an activation energy of '$E = 11.72e7$ mJ$(mol)^{-1}$'. Similarly, Shemet et al. [51] performed a kinetics analysis on 2D C/C composites in air at an atmospheric pressure and calculated an activation energy of '$E = 11.6e7$ mJ$(mol)^{-1}$'. Therefore, it is hypothesized that these variations in activation energies might be influenced by the fiber volume fraction, reactivity of carbon materials, fiber architecture and experimental conditions such as oxidizing medium, air flow rate and pressure [54,55].

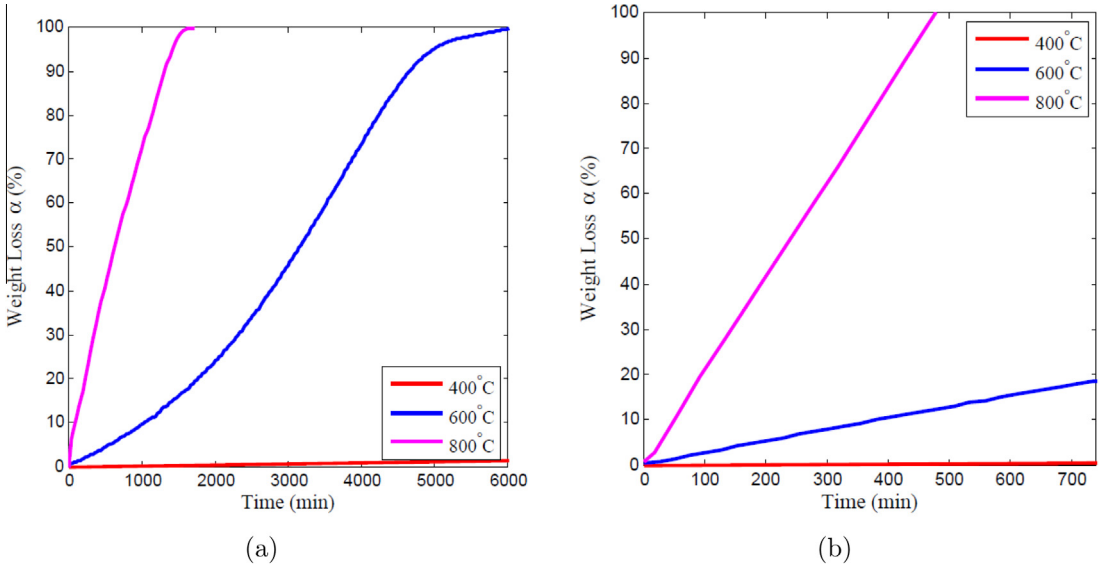


**Fig. 7.** (a) Predicted TG curves for the carbon fibers for temperatures ranging from 400 °C to 800 °C in steady air and (b) predicted TG curves for the carbon matrix for temperatures ranging from 400 °C to 800 °C in steady air.

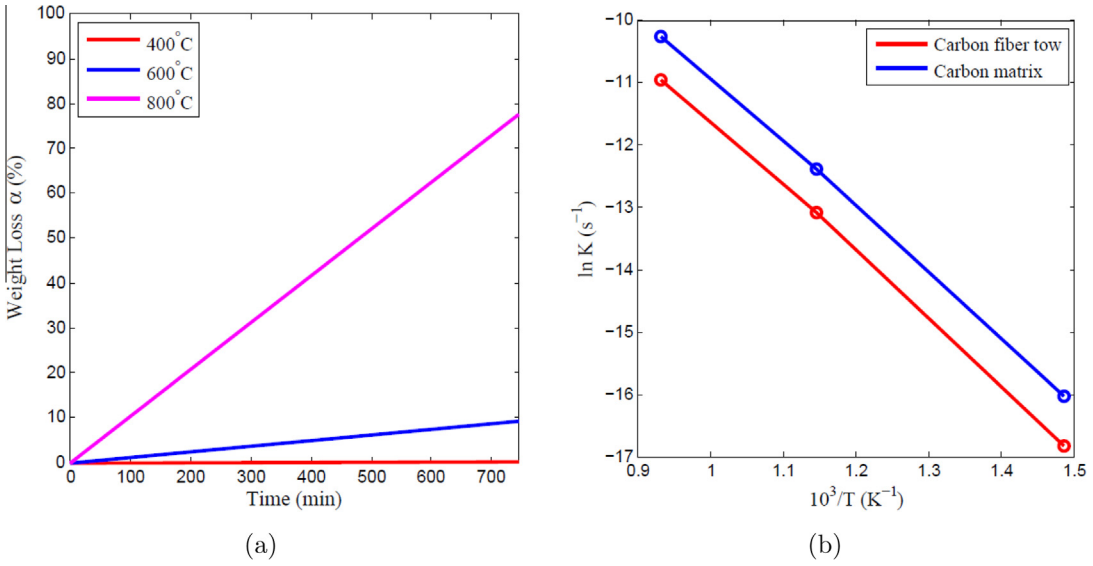


**Fig. 8.** (a) Predicted TG curves for the carbon fiber tows for temperatures ranging from 400 °C to 800 °C in steady air and (b) Arrhenius plots of oxidation of carbon fiber tow and carbon matrix assuming linear oxidation stage.

**Table 6**
Comparison of C/C composite kinetic parameters with the literature as a function of temperature and steady air conditions.

| Kinetic parameters | 400–800 °C |
|---|---|
| $A(s^{-1})$ C/C composite | 0.445 |
| $E(mJ * mol^{-1})$ C/C composite | 8.723e7 |
| $A(s^{-1})$ 2D C/C composite [46] | 1.57 |
| $E(mJ * mol^{-1})$ 2D C/C composite [46] | 8.563e7 |

Following this, the oxidation kinetics of the carbon fiber TG results (i.e., linear stage of Fig. 7(a)) are also analyzed and compared with the literature. The oxidation of PAN-based T300 carbon fibers consists of a single-step process through the whole range of temperatures with an activation energy of '$E = 9.01e7$ mJ$(mol)^{-1}$', whereas, Ismail [54] reported an activation energy of '$E = 9.41e7$ mJ$(mol)^{-1}$' for T300 carbon fibers at 100 ml/min in a temperature range of 600–950 °C. Likewise, Lamoroux et al. [39] reported an activation energy of '$E = 8e7$ mJ$(mol)^{-1}$' at 16.7 ml/min for temperatures in the range of 500–700 °C. It is shown that the activation energy of the carbon fibers considered in this paper is comparable to the values available from literature for flowing air and almost steady air conditions. Therefore, it is verified that the C/C composite and carbon fiber TG curves for steady conditions are in good correlation with previous literature as they are the most important inputs for the current analysis.

Finally, Fig. 8(b) shows the oxidation Arrhenius curves for both carbon fiber tow and matrix, which are also assumed to be linear through the whole range of temperatures. The corresponding kinetic parameters are listed in Table 7. The information provided to the computational model, i.e., weight loss with respect to temperature and time, is summarized by 3D surface plots for carbon fiber tows and matrix as shown in Fig. 9a) and (b), respectively.

## 7. Meso-scale model of the C/C composite

Macroscopic models have been developed from microscopic measurements by previous researchers [56–58,29]. A schematic representation of the meso-scale model developed to investigate the material considered in this work is shown in Fig. 10(a). Geometric information of the composite, such as, the tow width and thickness, individual layer thickness, etc. are required to create a meso-scale C/C composite voxel model using TexGen software. The tow thickness '$a$' and width '$b$' are $0.285 \pm 0.02$ mm and $2.55 \pm 0.07$ mm, respectively (Fig. 10(b)), as measured using an optical microscope (Model NJF-120A, OMAX Corporation, USA). The average thickness of the composite measured using a caliper is equal to $5.25 \pm 0.05$ mm. Thus, the approximate thickness of an individual layer is about 0.525 mm, since the composite consists of 10 layers. Other information, such as the desired mesh and weave pattern ($2 \times 2$ twill weave) are required to be specified in TexGen software.

Fig. 11 (a) and (b) show a $2 \times 2$ twill weave pattern from the top and orthogonal views of the homogenized tows. A voxel model of the meshed meso-scale C/C composite is imported into ABAQUS software that consists of fiber tows embedded in matrix material. Individual layer voxel model is stacked 10 times in the through-thickness direction and merged together to create the final meso-scale C/C composite model with sides equal to 10.56 mm and thickness of 5.25 mm (refer to Fig. 12(a)). The final model generated is an approximation of the 2D twill weave C/C composite with dimensions comparable to the test specimens analyzed in Leanos and Prabhakar [15].

## 8. Radiation heat transfer analysis

A radiation heat transfer analysis comprises the first step of the computational framework as shown in Fig. 2. This step consists of two phases: heating and decomposition. The heating phase is represented by conductive heat flux and the decomposition phase as heat flux in the form of gas. As explained by Bai et al. [59], the main mode of oxidation in fiber reinforced composites when exposed to high temperatures in air is a chemical reaction, which consists of four phases, i.e., heating, decomposition, ignition and combustion. In the current study, only heating and decomposition phases are considered in the oxidation model of the 2D C/C composite test specimens exposed to the experimental conditions described in Leanos and Prabhakar [15]. Besides this, convection and radiation heat are accounted for during the prediction of the thermal response of fiber-reinforced composites. However, since the air enclosed by the heating furnace is almost steady, the effect of heat transfer through convection on the thermal response is minimum. Therefore, only radiation heat flux '$q_{rad}$' is considered to be transferred from the furnace to the exposed composite surfaces (except the bottom surface). A schematic representation of the radiation heat transfer analysis within the C/C composite control volume is shown in Fig. 12(b). The solution of the heat transfer energy equation requires the specification of boundary conditions. In the experiments, the bottom surface of the composite is in contact with a ceramic boat, which is impermeable to heat and mass flux. Thus, this surface is assumed to be perfectly insulated, as shown in Fig. 2. On the other hand, surface radiation boundary conditions are defined on all the remaining surfaces of the meso-scale C/C composite unit cell. The heat flux due to radiation is governed by:

$$q_{rad} = \sigma\epsilon[(T_s - T^0)^4 - (T - T^0)^4] \tag{13}$$

where, '$q_{rad}$' is the heat flux on the exposed surfaces, '$\epsilon$' is the emissivity of the surfaces (i.e., $\epsilon = 0.9$), '$\sigma$' is the Stefan–Boltzmann constant (i.e., $5.67e-11$ mWmm$^{-2}$ K$^{-4}$), '$T_s$' is the temperature at every position and time on the surfaces, '$T$' is the temperature of the heating furnace walls (i.e., ambient temperature) at any time and '$T^0$' is the value of absolute zero (i.e., 0 K). The ambient temperature '$T$' is set to follow the thermal shock conditions from the experiments. In addition, the emissivity is suggested to be very close to that of an ideal black body and is assumed to be 0.9. For the initial boundary condition, the temperature distribution in the entire domain of the model at '$t = 0$' is set at room temperature ($T_{R.T.} = 25\,^{\circ}C$).

The transient heat transfer equation is numerically solved to determine the spatial and temporal distribution of temperature within the model domain during the thermal process. The equation is given by,

$$\frac{\partial}{\partial \underline{X}}\left(k(\underline{X})\frac{\partial T}{\partial \underline{X}}\right) + \dot{G} = C_p \rho \frac{\partial T}{\partial t} \tag{14}$$

where, the thermal conductivity '$k$', the density '$\rho$' and the specific heat capacity '$C_p$' are functions of space '$\underline{X}$'. '$\dot{G}$' is the heat generated due to the decomposition of the constituent materials into gases that are released to the exterior during the heating stage and is given by:

$$\dot{G} = \rho H_r \frac{\partial \alpha}{\partial t} \tag{15}$$

where, '$H_r$' and '$\alpha$' are the total heat generated and the weight loss due to oxidation, respectively. The heat generation '$\dot{G}$' is defined within ABAQUS using HETVAL subroutine, which is coupled with the computational framework to account for the heat flux in the form of gas. As a result, the numerical solution of Eq. (14) provides the weight loss, temperature and heat flux distribution with time and space within the model domain. Following this, the thermal response is coupled to stress analysis through a user material (UMAT) subroutine in order to relate the extent of weight loss with stiffness degradation, as explained in detail in Section 9.

During the decomposition step, it is considered that carbon material reacts with Oxygen enclosed within the heating furnace generating gases in form of CO and $CO_2$. In other words, when C/C composites are exposed to thermal shock conditions in air, they lose weight and heat flux is released from the composite surfaces (except the bottom side) to the exterior in the form of gas. Within the novel computational framework proposed here, the gases released to the exterior are accounted by the degree of decomposition (i.e., weight loss) of carbon that depends on temperature, time and position within the domain. The degree of decomposition for carbon material is obtained experimentally by Thermogravimetric analyses and the inputs to the computational model (i.e., kinetic parameters) are determined as explained in detail in Section 5. This information is critical for predicting the amount of weight loss of carbon fiber tows and carbon matrix in the model.

HETVAL subroutine is used to define the internal heat generated due to carbon material degradation (i.e., weight loss) within ABAQUS software. The kinetic parameters, '$A_i$' and '$E_i$' from Table 7, the density '$\rho$' for the carbon fiber tow and carbon matrix of Table 1 and the total heat generated '$Hr$' during isothermal oxidation are

**Table 7**
Kinetic parameters of carbon fiber tow and carbon matrix as a function of temperature and steady air conditions.

| Kinetic parameters | 400–800 °C |
|---|---|
| $A(s^{-1})$ Carbon fiber tow | 0.1990 |
| $E(mJ * mol^{-1})$ Carbon fiber tow | 8.6697e7 |
| $A(s^{-1})$ Carbon matrix | 0.6173 |
| $E(mJ * mol^{-1})$ Carbon matrix | 8.5117e7 |

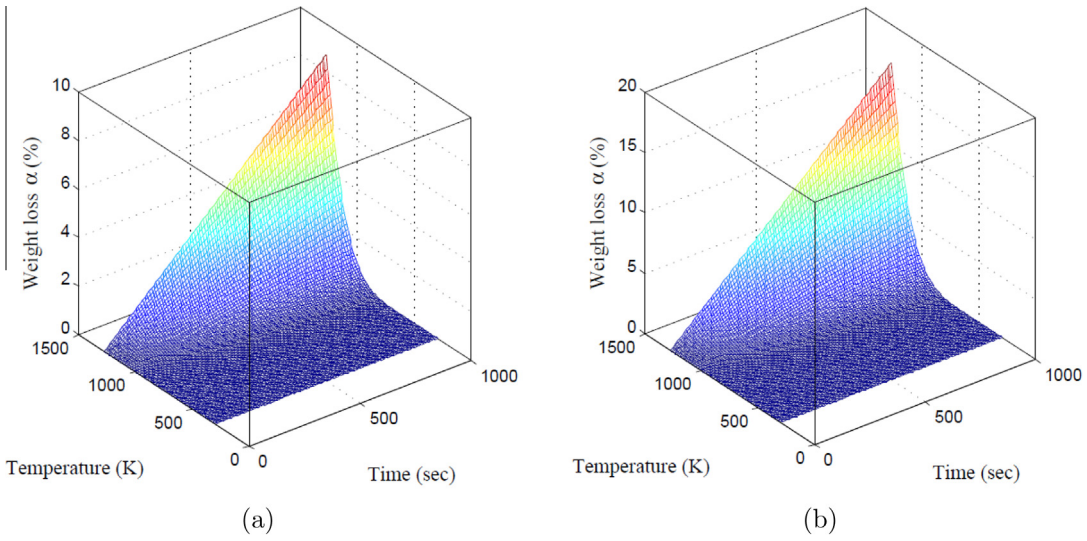


**Fig. 9.** 3D Surface plot of weight loss variation with time and temperature for (a) carbon fiber tows and (b) carbon matrix.

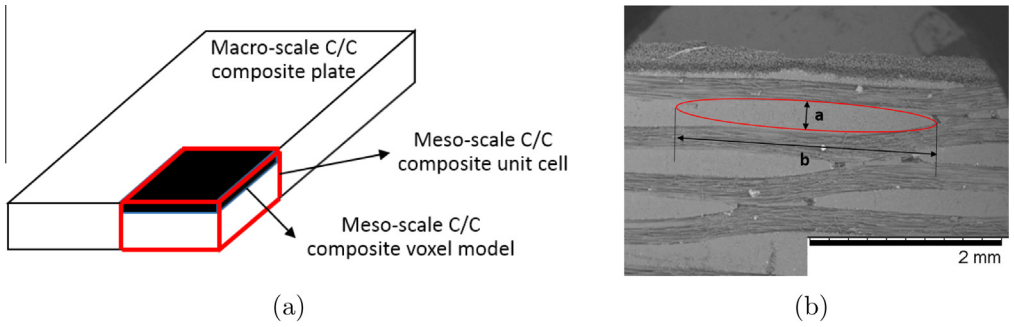


**Fig. 10.** (a) Upscaling approach to model the meso-scale C/C composite unit cell and (b) optical micrograph of a C/C composite transverse cross-section showing tow dimensions.

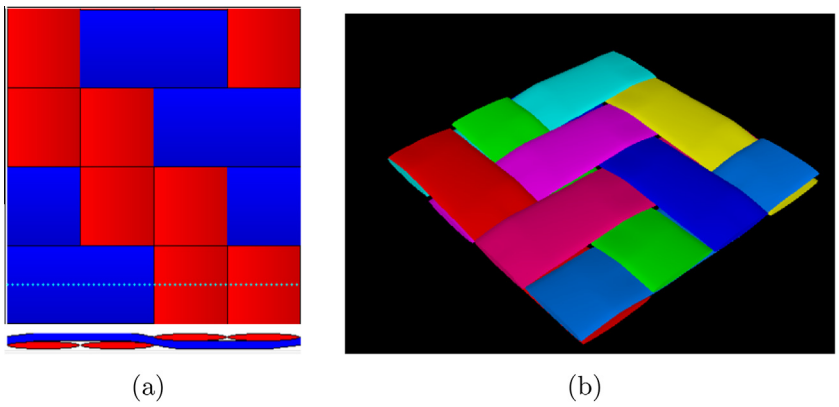


**Fig. 11.** TexGen voxel model of a single layer: (a) top view showing fiber architecture and (b) 3D view showing fiber tows interwoven together.

inputs to the HETVAL subroutine. The HETVAL subroutine is able to determine the extent of weight loss by specifying the Arrhenius equation from Eqs. (4) and (5) as:

$$\alpha_i = (DTIME * A_i^{\frac{-E_i}{T*R}}) + \alpha_i^0 \tag{16}$$

where '$\alpha$' is the weight loss, '*DTIME*' is the time increment, '*A*' and '*E*' are the kinetic parameters, '$\alpha^0$' is the weight loss from the previous step and subscript '*i*' defines the carbon fiber tow and carbon matrix material.

## 9. Stress analysis

Stress analysis comprises the second step of the computational framework (refer to Fig. 2) that is used for predicting the compressive stiffness of the pristine and thermally exposed C/C composite test specimens accounting for the carbon material degradation due to oxidation. In this study, a computational model replicating the through-thickness compression tests previously performed [15] is generated, where a through-thickness displacement boundary condition (i.e., $U_z = -0.00$ mm) is applied on the top surface of

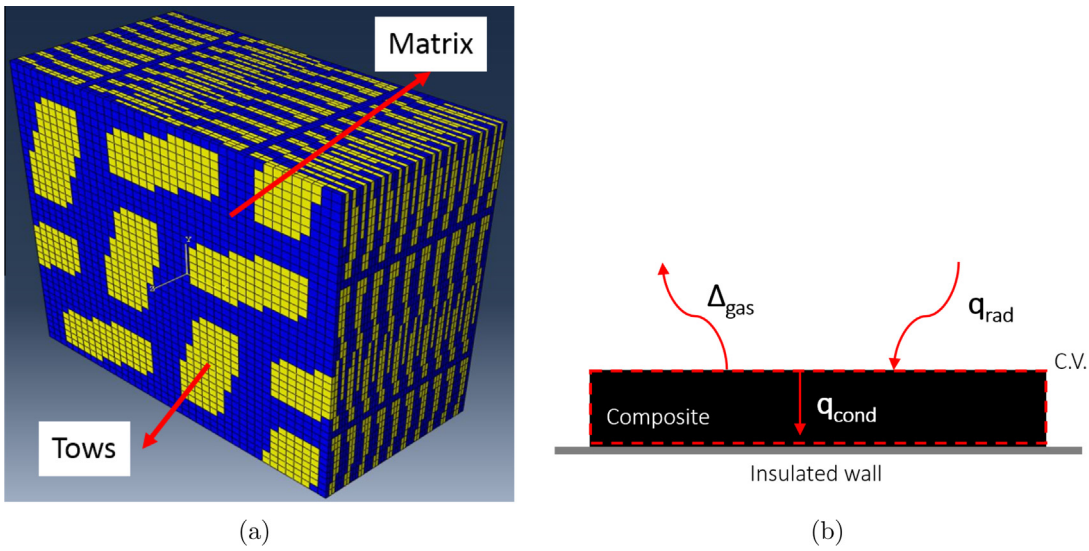


**Fig. 12.** (a) Meso-scale C/C composite unit cell with a total of 80,000 elements and (b) schematic representation of the radiation heat transfer analysis within the C/C composite control volume.

the meso-scale C/C composite unit cell with sides of 10.56 mm and thickness of 5.25 mm. Boundary conditions acting as roller supports are applied on the bottom surface, such that the model is free to expand in the in-plane direction due the through-thickness compressive load.The compressive stiffness is computed using the expression, '$E = \sigma\varepsilon$', where, '$\sigma$' is the stress applied and '$\varepsilon$' is the applied strain. '$\sigma$' is calculated by dividing the total force on the top surface by the top area of the unit cell ($A = 111.5136\ \text{mm}^2$) and $\varepsilon$ by dividing the displacement over its original thickness. The compressive stiffness is obtained for the meso-scale C/C composite unit cell under pristine and thermal shock conditions with temperatures ranging from 400 °C to 1000 °C in air and further compared to the experimental results.

In the experimental paper by Leanos and Prabhakar [15], it was concluded that the C/C composite compressive stiffness degrades at temperature as low as 400 °C in air due to oxidation. Hence, to account for this material degradation in the computational framework, a user material (UMAT) subroutine is coupled to a static analysis in ABAQUS. The UMAT is used to define the stiffness behavior of the composite constituent materials with respect to their corresponding weight loss. The components of the stiffness tensor '$E_i$' for tow and matrix are assumed to degrade linearly with the extent of weight loss '$\alpha_i$' as $E_i^{deg} = E_i(1 - \alpha_i)$, where '$E_i^{deg}$' is the degraded stiffness for both tow and matrix individually.

## 10. Results

The proposed computational framework is utilized to predict the oxidation behavior and the through-thickness compressive stiffness degradation of a C/C composite subjected to one cycle thermal shock condition and peak temperatures ranging from 400 °C to 1000 °C. The heat flux distribution within the composite meso-scale model is shown in Fig. 13 at the peak of the 800 °C thermal shock condition (i.e., $time = 3500$ s). In Fig. 13 (a) it is observed that heat is being propagated to the interior of the unit cell from the heated surfaces. A view of the temperature distribution within the interior of the composite is shown in Fig. 13 (b), where the bottom surface possesses the minimum amount of heat flux as it is assumed to be insulated, whereas maximum heat flux is concentrated at the matrix/tow interface due a mismatch of the constituents thermal conductivity. Also, the edges of the unit cell are more susceptible to the oxidation attack during the ablation process.

Fig. 14 shows the weight loss distribution within the model at the end of the 800 °C thermal shock process (i.e., $time_{end} = 20,700$ s), where the constituent weight loss is maximum. In this figure, it is verified that the carbon matrix is more reactive than the carbon fiber tows, since the carbon matrix degrades much faster than the fiber tows as noticed in Leanos and Prabhakar [15]. The maximum amount of weight loss for the carbon fiber tows and carbon matrix within the domain at the end of each thermal cycle (i.e., from 600 °C to 1000 °C) is tabulated in Table 8, where it is observed that the maximum constituent weight loss increases with increasing thermal shock peak temperature.

Further, by calculating the average temperature at the left and right surfaces at a given time, it is found that the temperature difference through the thickness direction reaches a maximum value of 0.005 °C. Therefore, the temperature distribution is assumed to be uniform throughout the domain. This behavior is due to the high thermal conductivity of the carbon material and the high temperatures that are being applied.

The average pristine compressive stiffness of the unit cell is predicted to be 1.8 GPa, which has about 0.03% of difference as compared to that obtained experimentally (i.e., 1.74 GPa) [15] as shown by the blue line in Fig. 15. Next, the compressive stiffness is predicted upon exposure to thermal shock conditions with temperatures ranging from 400 °C to 1000 °C and is further compared to that obtained experimentally [15] (refer to Fig. 15). In this figure, the compressive response for the 400 °C thermal shock condition is assumed to be the same as the pristine compressive stiffness since the material degradation for this case is minimum. Fig. 15 shows that the experimental and predicted compressive responses decrease with increasing thermal shock peak temperature. However, the compressive stiffness obtained by the proposed model (red curve) tends to overpredict the experimental stiffness (black curve) and is attributed to the complexity of replicating the experimental conditions (e.g., air flow rate). Further, the percentage difference between the predicted and experimental stiffness values is calculated as shown in Table 9, where the maximum percentage difference is found for the 800 °C thermal shock condition and is about 37.67%. It can be observed that this percentage difference has been reduced by half as compared to that calculated when using flowing air conditions (i.e., 80%). Also, this large percentage error might be due to the existence of more than one single-step processes in the Arrhenius curve, however, more input TG curves

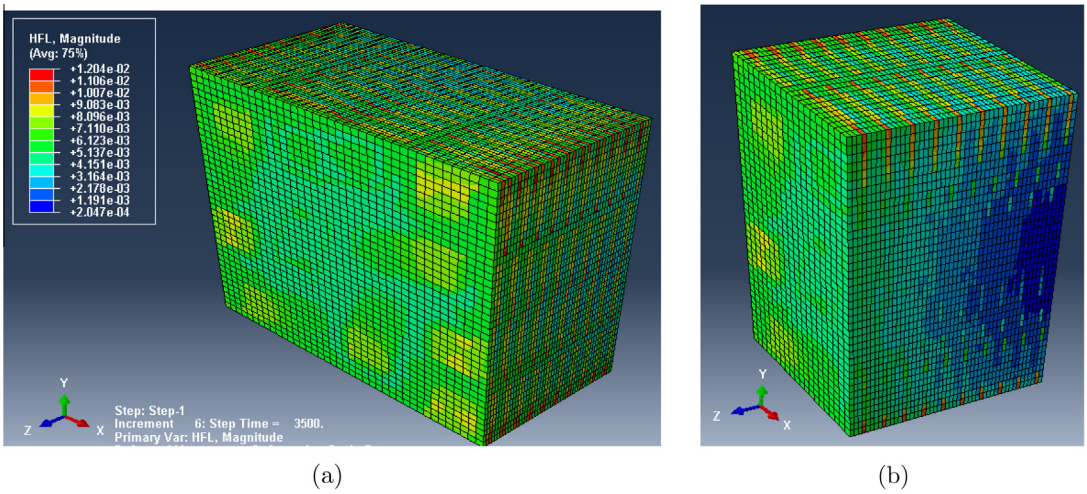


**Fig. 13.** Different views of the heat flux distribution within the meso-scale C/C composite unit cell at the peak of the 800 °C thermal shock condition: (a) whole model (b) interior cut.

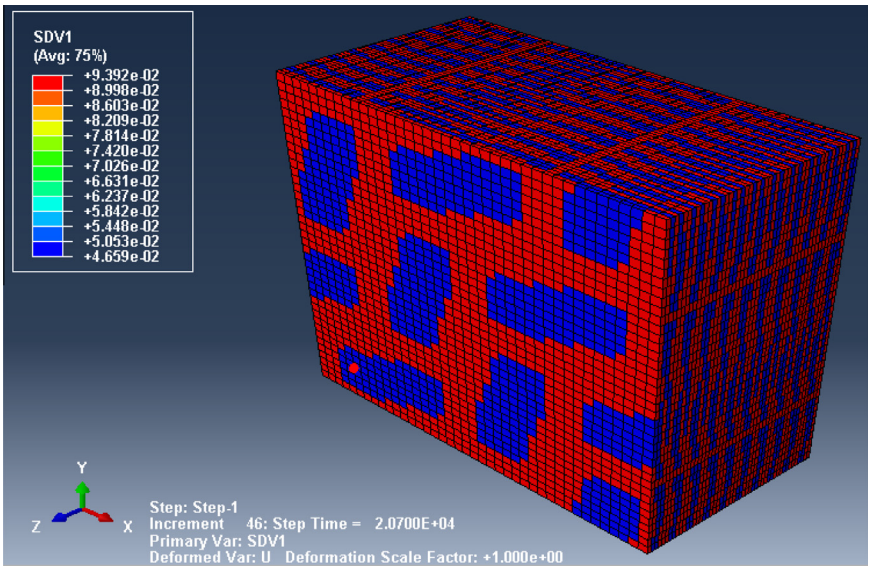


**Fig. 14.** Weight loss distribution within the C/C composite model domain at the end of the 800 °C thermal shock condition.

**Table 8**
Maximum values of weight loss for the carbon constituents within the model domain at the end of individual thermal shock conditions.

| Weight loss α (%) | 600 °C | 700 °C | 800 °C | 1000 °C |
|---|---|---|---|---|
| Fiber tow | 0.39 | 1.52 | 4.66 | 26.4 |
| Matrix | 0.83 | 3.11 | 9.39 | 51.74 |

are required to verify this hypothesis. Since, the percentage difference obtained for the other thermal shock conditions is less than 11.55%, it is concluded that the proposed computational technique offers good correlation between computational and experimental results for temperatures below 700 °C.

To summarize, a transient radiation heat transfer and static stress analyses are developed within the finite element method framework to predict the experimental tests and results [15], and a valid benchmark for the calculation of extent of weight loss and through-thickness compressive stiffness degradation of C/C composites under thermal shock conditions in air is provided.

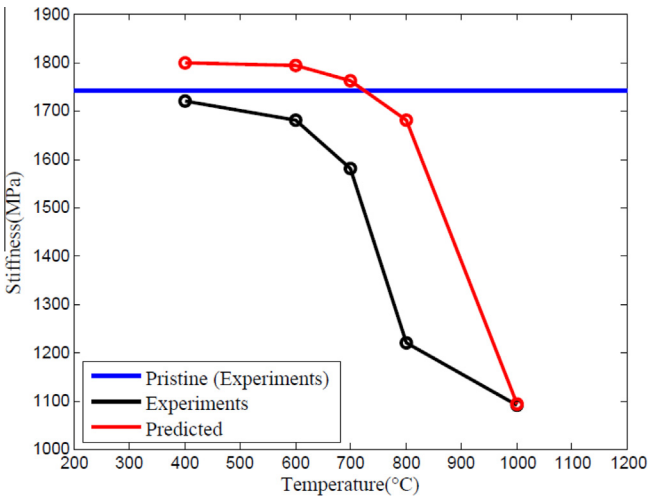


**Fig. 15.** Compressive stiffness degradation of the meso-scale C/C composite unit cell after being exposed to thermal shock conditions.

**Table 9**
Calculated percentage of error between experimental and predicted stiffness responses.

| Thermal shock condition | 400 °C | 600 °C | 700 °C | 800 °C | 1000 °C |
|---|---|---|---|---|---|
| Percentage of error (%) | 4.65 | 6.69 | 11.55 | 37.67 | 0.21 |

## 11. Concluding remarks

A three-dimensional finite element framework is developed in this paper to predict the effects of oxidation on the compressive properties of C/C composites subjected to thermal shock conditions. The temperature dependent thermo-physical property i.e., percentage weight loss, can be obtained in space and time domain using this model. It is concluded that the thermal response of a C/C composite can be modeled using a meso-scale representative unit cell, whose physical morphology is based on microscopic measurements. Also, the modeling framework proposed in this work provides good predictions of the amount of weight loss and stiffness degradation of the 2D woven C/C composites during thermal shock conditions in air, resulting in good agreement with experimental data [15] for temperatures below 700 °C. It is expected that this modeling technique can be further applied to composite materials with complex architectures with known material parameters and fiber volume fraction. Furthermore, it can be used for virtual testing for other 2D C/C composites with similar fiber architecture in the early stages of design, thus, minimizing the cost and time associated with conducting physical experiments on composites to ensure their good performance in many high temperature structural applications.

## Acknowledgements

The authors would like to thank Dr. Evgeny Shafirovich and his students Mr. Alan Esparza and Mr. Armando Delgado from the Mechanical Engineering Department at the University of Texas at El Paso (UTEP) for assisting with the TG experiments presented in this paper. The authors would also like to acknowledge Dr. José Guadalupe Chacón Nava and the doctoral student Mr. Gregorio Vázquez Olvera from Centro de Investigación en Materiales Avanzados, S.C. (CIMAV) for assisting with thermogravimetric analysis on C/C composite specimens.

## References

[1] Naslain R. Design, preparation and properties of non-oxide cmcs for application in engines and nuclear reactors: an overview. Compos Sci Technol 2004;64(2):155–70.
[2] Mohamed S, Hiroshi H, Shuichi W, Mitsuhiro W. K.M., Comparison of 2d and 3d carbon/carbon composites with respect to damage and fracture resistance. Carbon 2003;41(5):1069–78. http://dx.doi.org/10.1016/S0008-6223(02)00442-6.
[3] Evans A, Zok F. Review. the physics and mechanics of fibre-reinforced brittle matrix composites. J Mater Sci 1994;29(15):3857–96.
[4] Heredia F, Spearing S, Mackin T, He M, Evans A, Mosher P, Brandsted P. Notch effects in carbon matrix composites. J Am Ceram Soc 1994;77(11):2817–27. http://dx.doi.org/10.1111/j.1151-2916.1994.tb04510.x.
[5] Mackin T, Purcell T, He M, Evans A. Notch sensitivity and stress redistribution in three ceramic-matrix composites. J Am Ceram Soc 1995;78(7):1719–28. http://dx.doi.org/10.1111/j.1151-2916.1995.tb08881.x.
[6] Cady C, Heredia F, Evans A. In-plane mechanical properties of several ceramic-matrix composites. J Am Ceram Soc 1995;78(8):2065–78. http://dx.doi.org/10.1111/j.1151-2916.1995.tb08618.x.
[7] He M, Wu B, Suo Z. Notch-sensitivity and shear bands in brittle matrix composites. Acta Metall Mater 1994;42(9):3065–70. http://dx.doi.org/10.1016/0956-7151(94)90403-0.
[8] Jian W, Mototsugu S. The crack-face fiber bridging of a 2d-c/c-composite. Carbon 1996;34(3):387–95.
[9] Hatta H, Denk L, Watanabe T, Shiota I, Aly-Hassan M. Fracture behavior of carbon–carbon composites with cross-ply lamination. J Compos Mater 2004;38(17):1479–94.
[10] Goto K, Hatta H, Takahashi H, Kawada H. Effect of shear damage on the fracture behavior of carbon-carbon composites. J Am Ceram Soc 2001;84(6):1327–33. http://dx.doi.org/10.1111/j.1151-2916.2001.tb00837.x.
[11] Lars D, Hiroshi H, Akihiro M, Satoshi S. Shear fracture of c/c composites with variable stacking sequence. Carbon 2001;39(10):1505–13.
[12] Chollon G, Siron O, Takahashi J, Yamauchi H, Maeda K, Kosaka K. Microstructure and mechanical properties of coal tar pitch-based 2d-c/c composites with a filler addition. Carbon 2001;39(13):2065–75.
[13] Sines G, Zheng Y, Vickers B. Creep of carbon yarn and a carbon-carbon composite at high temperatures and high stresses. Carbon 1989;27(3):403–15. http://dx.doi.org/10.1016/0008-6223(89)90073.
[14] Sato S, Kurumada A, Iwaki H, Komatsu Y. Tensile properties and fracture toughness of carbon-fiber felt reinforced carbon composites at high temperature. Carbon 1989;27(6):791–801. http://dx.doi.org/10.1016/0008-6223(89)90029-8.
[15] Leanos A, Prabhakar P. Experimental investigation of thermal shock effects on carbon-carbon composites. Compos Struct 2015;132:372–83. http://dx.doi.org/10.1016/j.compstruct.2015.05.038.
[16] Liu N, Yang Q, Micromechanical modeling and numerical simulation of ablation of 3d c/c composites. In: ICF13; 2013.
[17] Bacos M. Carbon-carbon composites, oxidation behavior and coatings protection. J Phys IV 1993;3(7):1895–903.
[18] Manocha L. High performance carbon–carbon composites. Sadhana 2003;28(1–2):349–58. http://dx.doi.org/10.1007/bf02717143.
[19] Nathan R, Modeling of ablation of carbon–carbon composite thermal protection system. In: Collection of technical papers-39th AIAA thermophysics conference, vol. 2, 2007, p. 1307–14.
[20] Zhongping L. Major advancement and development trends in studyof hot-wall microwave-transparency mechanisms and high-temperature microwave-transparent materials. Mater Chin 2013;4:002.
[21] Zhao J, Bradt R, Walker Jr P. Effect of air oxidation at 873 k on the mechanical properties of a carbon–carbon composite. Carbon 1985;23(1):9–13. http://dx.doi.org/10.1016/0008-6223(85)90189-7.
[22] Weisshaus H, Kenig S, Sivegmann A. Effect of materials and processing on the mechanical properties of c/c composites. Carbon 1991;29(8):1203–20.
[23] Dillon F, Thomas K, Marsh H. The influence of matrix microstructure on the mechanical properties of cfrc composites. Carbon 1993;31(8):1337–48. http://dx.doi.org/10.1016/0008-6223(93)90095-R.
[24] Bai Y, Valle T, Keller T. Modeling of thermo-physical properties for frp composites under elevated and high temperature. Compos Sci Technol 2007;67(15–16):3098–109.
[25] Aspa Y, Quintard M, Plazanet F, Descamps C, Vignoles G. Ablation of carbon/carbon composites: direct numerical simulation and effective behavior. In: Mechanical Properties and Performance of Engineering Ceramics and Composites: Ceramic Engineering and Science Proceedings, vol. 26, No. 2. John Wiley & Sons Inc.; 2008. p. 99–106.
[26] Vignoles GL, Lachaud J, Aspa Y, Quintard M. Effective surface recession laws for the physico-chemical ablation of C/C composite materials. In: Mechanical Properties and Performance of Engineering Ceramics and Composites V: Ceramic Engineering and Science Proceedings, vol. 31. John Wiley & Sons Inc.; 2010. p. 351–60.
[27] Lachaud J, Vignoles GL, Goyhnche J-M, Epherre J-F. Ablation in carbon/carbon composites: microscopic observations and 3D numerical simulation of surface roughness evolution. In: Interfaces in Heterogeneous Ceramic Systems: Ceramic Transactions Series, vol. 191. John Wiley & Sons Inc.; 2011. p. 147–60.
[28] Laborde P, Toson B, Odunlami M. High temperature damage model for carbon-carbon composites. Eur J Mech – A/Solids 2011;30(3):256–68. http://dx.doi.org/10.1016/j.euromechsol.2010.12.014.
[29] Farooqi J, Sheikh M. Finite element modelling of thermal transport in ceramic matrix composites. Comput Mater Sci 2006;37(3):361–73.
[30] Sheikh M, Taylor S, Hayhurst D, Taylor R. Microstructural finite-element modelling of a ceramic matrix composite to predict experimental measurements of its macro thermal properties. Modell Simul Mater Sci Eng 2001;9(1):7.
[31] Pardini L, Gregori M. Modeling elastic and thermal properties of 2.5D carbon fiber C/SiC hybrid matrix composites by homogenization method. J Aerosp Technol Manage 2010;2:183–94. http://dx.doi.org/10.5028/jatm.2010.02026510.
[32] Guo W, Xiao H, Yasuda E, Cheng Y. Oxidation kinetics and mechanisms of a 2d-c/c composite. Carbon 2006;44(15):3269–76.
[33] Vyazovkin S, Wight C. Model-free and model-fitting approaches to kinetic analysis of isothermal and nonisothermal data. Thermochim Acta 1999;340–341:53–68.
[34] Guo W, Xiao H. Mechanisms and modeling of oxidation of carbon felt/carbon composites. Carbon 2007;45(5):1058–65.
[35] Park S, Seo M. The effects of $mosi_2$ on the oxidation behavior of carbon/carbon composites. Carbon 2001;39(8):1229–35.
[36] Halbig M, Cawley J. Modeling the oxidation kinetics of continuous carbon fibers in a ceramic matrix. Tech. rep., DTIC Document; 2000.
[37] Goujard S, Vandenbulcke L, Tawi H. The oxidation behaviour of two- and three-dimensional c/sic thermostructural materials protected by chemical-vapour-deposition polylayers coatings. J Mater Sci 1994;29(23):6212–20. http://dx.doi.org/10.1007/BF00354562.
[38] Lamouroux F, Camus G, Thebault J. Kinetics and mechanisms of oxidation of 2d woven c/sic composites: I, experimental approach. J Am Ceram Soc 1994;77(8):2049–57.

[39] Lamouroux F, Bourrat X, Nasalain R, Sevely J. Structure/oxidation behavior relationship in the carbonaceous constituents of 2d-c/pyc/sic composites. Carbon 1993;31(8):1273–88.
[40] Filipuzzi L, Camus G, Naslain R, Thebault J. Oxidation mechanisms and kinetics of 1d-sic/c/sic composite materials: I, an experimental approach. J Am Ceram Soc 1994;77(2):459–66.
[41] Li T, Zheng X. Oxidation behaviour of matrix-modified carbon-carbon composites at high temperature. Carbon 1995;33(4):469–72.
[42] Dačić B, Marinković S. Kinetics of air oxidation of unidirectional carbon fibres/cvd carbon composites. Carbon 1987;25(3):409–15.
[43] Han J, He X, Du S. Oxidation and ablation of 3d carbon–carbon composite at up to 3000 c. Carbon 1995;33(4):473–8.
[44] McKee D. Oxidation behavior and protection of carbon/carbon composites. Carbon 1987;25(4):551–7. http://dx.doi.org/10.1016/0008-6223(87)90197-7.
[45] Luo R, Cheng J, Wang T. Oxidation behavior and protection of carbon/carbon composites prepared using rapid directional diffused cvi techniques. Carbon 2002;40(11):1965–72.
[46] Hatta H, Fukuda H, Goto K, Oxidation behavior modeling of ceramic coated carbon/carbon composites. In: Proceeding of the twelfth international conference on composite materials; 1999.
[47] Henderson J, Wiebelt J, Tant M, Moore G. A method for the determination of the specific heat and heat of decomposition of composite materials. Thermochim Acta 1982;57(2):161–71. http://dx.doi.org/10.1016/0040-6031(82)80057-9.
[48] Fanucci JP. Thermal response of radiantly heated kevlar and graphite/epoxy composites. J Compos Mater 1987;21(2):129–39.
[49] Craig T. (Ph.D. thesis). Lausanne.
[50] Cheng L, Xu Y, Zhang L, Yin X. Oxidation behavior of carbon–carbon composites with a three-layer coating from room temperature to 1700c. Carbon 1999;37(6):977–81. http://dx.doi.org/10.1016/S0008-6223(98)00293-0.
[51] Shemet V, Pomytkin A, Neshpor V. High-temperature oxidation behaviour of carbon materials in air. Carbon 1993;31(1):1–6.
[52] McKee D. Oxidation behavior of matrix-inhibited carbon/carbon composites. Carbon 1988;26(5):659–64. http://dx.doi.org/10.1016/0008-6223(88)90068-1.
[53] McKee D. Borate treatment of carbon fibers and carbon/carbon composites for improved oxidation resistance. Carbon 1986;24(6):737–41. http://dx.doi.org/10.1016/0008-6223(86)90183-1.
[54] Ismail I. On the reactivity, structure, and porosity of carbon fibers and fabrics. Carbon 1991;29(6):777–92.
[55] Eckel A, Cawley J, Parthasarathy T. Oxidation kinetics of a continuous carbon phase in a nonreactive matrix. J Am Ceram Soc 1995;78(4):972–80.
[56] Nicoletto G, Riva E. Failure mechanisms in twill-weave laminates: fem predictions vs. experiments. Compos Part A 2004;35(7–8):787–95. http://dx.doi.org/10.1016/j.compositesa.2004.01.007.
[57] Woo K, Goo N. Thermal conductivity of carbon-phenolic 8-harness satin weave composites. Compos Struct 2004;66(1):521–6.
[58] Zako M, Uetsuji Y, Kurashiki T. Finite element analysis of damaged woven fabric composite materials. Compos Sci Technol 2003;63(3):507–16.
[59] Bai Y, Vallée T, Keller T. Modeling of thermal responses for frp composites under elevated and high temperatures. Compos Sci Technol 2008;68(1):47–56.